ELSEVIER

Catalysis Today 81 (2003) 137–148

CATALYSIS TODAY

www.elsevier.com/locate/cattod

Correlation of alkane oxidation performance with STM and tunneling spectroscopy measurements of heteropolyacid catalysts

In K. Song [a,1], James E. Lyons [b], Mark A. Barteau [a,*]

[a] *Department of Chemical Engineering, Center for Catalytic Science and Technology, University of Delaware, Newark, DE 19716, USA*
[b] *The Catalyst Group, P.O. Box 637, Spring House, PA 19477, USA*

Abstract

A comprehensive study of the surface electronic properties of nanostructured heteropolyacid (HPA) monolayers was carried out using scanning tunneling microscopy (STM) with the aim of developing tools for rational selection of HPAs as oxidation catalysts. A wide set of Keggin-type HPAs with different counter-cation, framework polyatom, and central heteroatom substitutions were examined. HPA samples deposited on graphite surfaces formed two-dimensional well-ordered monolayer arrays, and exhibited negative differential resistance (NDR) behavior in their tunneling spectra. Substitution of more electronegative atoms for counter-cations or for the central heteroatom shifted the NDR peaks to less negative voltages, corresponding to increased reduction potentials of the HPAs. However, substitution of more electronegative framework polyatoms shifted the NDR peaks to more negative voltages, corresponding to decreased reduction potentials. Irrespective of the exchanged/substituted positions, it was consistently observed that NDR peaks appeared at less negative potentials for higher reduction potentials of the HPAs, across all families of HPAs examined in this work. The NDR peak voltage could be utilized as a correlating parameter (as an alternative parameter) for the reduction potential; a less negative NDR peak voltage corresponds to a higher reduction potential of the HPA. A "volcano" plot constructed for the first time by relating NDR peak voltage to catalytic performance of HPAs in propane oxidation (a target reaction) showed that there was an optimum range of NDR peak voltages for the best performance in this reaction. The ability to tune NDR peak voltages of HPAs by exchange/substitution can be a strong advantage in designing HPAs in a systematic way as selective oxidation catalysts. This work has successfully demonstrated that NDR peak voltages of HPAs can serve as selection, prediction, and design tools in identifying efficient HPAs for propane oxidation.

Keywords: Heteropolyacid; Scanning tunneling microscopy; Tunneling spectroscopy; Selective alkane oxidation

1. Introduction

Scanning tunneling microscopy (STM) has shown tremendous potential for surface and interface analyses on a nanometer scale [1], and has provided direct insights to chemical reactions on metal surfaces [2]. Direct imaging of adsorbed molecules on catalyst surfaces is of great importance in understanding chemical reaction pathways and reaction sites on surfaces.

* Corresponding author. Tel.: +1-302-831-8905; fax: +1-302-831-8201.
E-mail address: barteau@che.udel.edu (M.A. Barteau).
[1] Present address: Department of Environmental and Applied Chemical Engineering, Kangnung National University, Kangnung 210-702, Korea.

0920-5861/03/$ – see front matter © 2003 Elsevier Science B.V. All rights reserved.
doi:10.1016/S0920-5861(03)00107-X

Examples of reactive adsorbates imaged include carbon monoxide on Rh(1 1 1) [3] and Ag(1 1 0) [4]; oxygen on Pd(1 1 1) [5] and Pt(1 1 1) [6]; benzoic acid on Cu(1 1 0) [7]; *m*-xylene and *p*-xylene on Pd(1 1 1) [8]; and methoxy and formate species on Cu(1 1 0) [9]. An STM image contains both geometric and electronic information about the sample. Highly resolved STM images can be directly utilized to distinguish between different molecules with very similar geometric structures and molecular sizes. For example, products from the reaction of chlorine with Si(1 1 1) (7 × 7) surfaces have been distinguished by their registries and sizes [10], metal atoms on an alloy surface have been distinguished by their apparent height difference [11], and metal phthalocyanines on Au(1 1 1) have been identified by metal d-orbital occupation-dependent images [12]. On the other hand, tunneling spectroscopy (TS) probes only electronic states of surface species, and has also been utilized as a valuable technique to distinguish between chemically inequivalent sites or adsorbates with nearly identical geometric structures and sizes [13]. The distinction is made based on differences in electronic structures. Tunneling spectra measured for a single organic molecule on a metal surface, e.g. C_2H_2 on Cu(1 0 0), have also proven to be a valuable method to identify adsorbates [14]. Recently, the so-called negative differential resistance (NDR) phenomenon, a distinctive current–voltage (*I*–*V*) behavior frequently observed in semiconducting or insulating materials [15,16], was reported in a molecular device involving two C_{60} molecules [17] and in self-assembled monolayers of electroactive thiols on gold [18], as well as in our studies of heteropolyacid (HPA) monolayers [19–25].

Heteropolyacids are early transition metal–oxygen anion clusters that exhibit a wide range of molecular sizes, compositions, and architectures [26]. Among various HPA structural classes, the Keggin-type [27] HPAs have been widely employed as catalysts in homogeneous and heterogeneous systems for acid–base and oxidation reactions [28–30]. One of the great advantages of HPA catalysts is that their catalytic properties can be tuned by changing the identity of charge-compensating counter-cations, heteroatoms, and framework metal atoms (polyatoms) [31]. Previous STM studies have demonstrated that HPAs deposited on graphite surfaces form two-dimensional well-ordered arrays [32,33] and exhibit negative differential resistance in their tunneling spectra [19–25]. Simple one-dimensional theory predicts that the transmission probability between two electronically equivalent electrodes should increase monotonically with increasing applied potential. The NDR phenomenon in tunneling spectra of HPAs is a consequence of a double-barrier resonant tunneling structure or quantum well in which the electron transmission probability increases with increasing applied potential at a resonance (or defect or trap state) energy level, and has been observed consistently for the arrays of pure HPAs [19–25]. A similar explanation for NDR observed for an Anderson-type $[PtMo_6O_{24}]^{4-}$ HPA was also recently offered [34]. The NDR feature at spatially well-resolved positions in the HPA arrays can be utilized as a tool to distinguish structurally identical but electronically different molecules in mixed HPA arrays on a site-by-site basis, for example, individual molecules of soccer ball-like $H_3PW_{12}O_{40}$ and $H_3PMo_{12}O_{40}$ in a mixed array [35]. We have shown that NDR peak voltages of HPAs are closely related to the electronic properties of HPAs and, in turn, to the redox potentials of HPAs [19–23]. NDR peak voltages can be influenced by the identity of the counter-cations [19–22], framework transition metal atoms [20–22], heteroatoms [23], and adsorbed organic molecules [23–25].

Reported in this work is a comprehensive investigation of surface chemical and electronic properties of nanostructured HPA monolayers probed by STM for rational design of HPAs as selective oxidation catalysts. A wide set of Keggin-type [27] HPAs with different counter-cation, polyatom, and heteroatom substitutions were examined. HPA samples were deposited on a highly oriented pyrolytic graphite (HOPG) surface in order to obtain images and tunneling spectra. The observed NDR peak voltages of HPA monolayers were correlated with the redox properties of the HPAs. Such a level of surface characterization may offer the prospect of using simple STM measurements on HPAs in air as predictive tools in oxidation catalysis. With NDR peak voltages as a correlating parameter, we attempted for the first time to construct "volcano" plots to correlate and to predict desired selective oxidation performance. The aim of these plots is to provide a design/selection basis for HPAs by defining the optimum range of reduction potentials/NDR peak voltages required for a given oxidation reaction.

Selective oxidation of propane to acrylic acid (AA) was chosen as the prototype reaction in this work. This reaction, together with oxidation of isobutane into methacrylic acid, has attracted much attention in the chemical industry because of the economic advantage of utilizing cheaper alkane feedstocks. Several alternative families of catalysts have been explored so far for propane oxidation. These include vanadyl pyrophosphate [36], multifunctional metal oxides [37–39], and HPAs [36,40–44]. The multifunctional metal oxides typically contain oxides of molybdenum and vanadium along with elements such as niobium, antimony, and tellurium, for example $Mo_1V_{0.3}Te_{0.23}Nb_{0.12}O_n$ [37,38] and $Mo_1V_{0.3}Te_{0.25}Nb_{0.1}O_n$ [39]. The HPAs are largely based on acid, alkali, or pyridinium forms of phosphomolybdate Keggin ions, $[PMo_{12}O_{40}]^{3-}$, and transition metal (V or Fe)-substituted variants of these, for example $H_5PMo_{10}V_2O_{40}$ [36], $Cs_{2.5}Fe_{0.08}H_{1.26}PMo_{11}V_1O_{40}$ [42], $H_2(VO)_{0.5}PMo_{12}O_{40}/Cs_3PMo_{12}O_{40}$ [43], and $H_4PMo_{11}V_1O_{40}{\cdot}4Ta_2O_5$ [44]. It is expected that a systematic step-by-step approach, based on surface electronic properties of nanostructured HPA monolayers, to quantify tunable redox properties of HPAs will be useful to establish a rational strategy for the selection of HPA catalysts efficient for propane oxidation and other desired oxidation processes.

2. Experimental

2.1. Sample preparation and deposition

A wide set of the following HPA families were examined: cation-exchanged $RPMo_{12}O_{40}$ (R = H_3, Cs_3, $Co_{3/2}$, Bi_1, $H_1(VO)_1$, $H_{0.8}Cu_{0.1/2}Sb_{0.1/3}(VO)_1$, etc.) and $RPMo_{11}V_1O_{40}$ (R = H_4, $H_{3.8}Cu_{0.1/2}Bi_{0.1/3}$); polyatom-substituted $H_{3+x}PMo_{12-x}V_xO_{40}$ ($x = 0$–3) and $H_{3+x}PW_{12-x}V_xO_{40}$ ($x = 0$–3); heteroatom-substituted $H_nXW_{12}O_{40}$ (X = P(V), Si(IV), B(III), Co(II)) and $H_nXMo_{12}O_{40}$ (X = As(V), P(V), Si(IV)) HPAs. Commercially available $H_3PMo_{12}O_{40}$, $H_3PW_{12}O_{40}$, $H_4SiW_{12}O_{40}$, $H_4SiMo_{12}O_{40}$, and $H_{3+x}PW_{12-x}V_xO_{40}$ ($x = 1$–3) samples were purchased from Aldrich and Nippon Inorganic Color and Chemical Co. $H_5BW_{12}O_{40}$ and $H_6CoW_{12}O_{40}$ were provided by Prof. Craig L. Hill at Emory University (Atlanta, GA). $H_{3+x}PMo_{12-x}V_xO_{40}$ ($x = 1$–3) HPAs were supplied by Dr. K. Kourtakis at E.I. duPont de Nemours and Company (Wilmington, DE). $H_3AsMo_{12}O_{40}$ was prepared according to methods in the literature [26,45]. Cation-exchanged HPAs were prepared by replacing some or all protons with metal atoms or vanadyl species, according to published methods [46–48]. Nominal 0.01 M aqueous solutions of each HPA sample were prepared. A drop of solution was deposited on a freshly cleaved HOPG surface and allowed to dry in air for ca. 1 h at room temperature for STM imaging and TS measurements. In the case of "insoluble" HPAs such as $Cs_3PMo_{12}O_{40}$, the liquid remained cloudy during the preparation, consistent with the formation of a suspension of fine particles, rather than a homogeneous solution. However, only ca. 10^{13} Keggin ions are required to form monolayers for imaging and spectroscopy measurements [13], suggesting that very limited extents of dissociation of the salts in solution may be sufficient. We have previously obtained both STM images and tunneling spectra for a variety of both soluble and nominally insoluble HPA salts by this method [19–25,32].

2.2. Scanning tunneling microscopy and tunneling spectroscopy

STM images were obtained in air using a Topometrix TMX 2010 instrument. Mechanically formed $Pt_{0.9}/Ir_{0.1}$ tips were used as probes. Scanning was done in the constant current mode at a positive sample bias of 100 mV and tunneling current of 1–2 nA. Tunneling spectra were measured in air. Both Topometrix TMX 2010 and LK Technologies LK-1000 STM instruments were used to confirm consistency and reproducibility of tunneling spectra. STM tips were first calibrated by imaging bare HOPG to confirm its standard periodicity (2.46 Å), and then the tips were moved to the HPA-covered section to image and obtain tunneling spectra of the HPA sample. To measure a tunneling spectrum, the sample bias was ramped from −2 to +2 V with respect to the tip and the tunneling current was monitored. The voltage axis in the tunneling spectrum represents the potential applied to the sample relative to that of the tip. TS measurements were performed at least 10–30 times each using at least three different tips for each sample to obtain more accurate and reproducible results, and to provide a basis for statistical analyses.

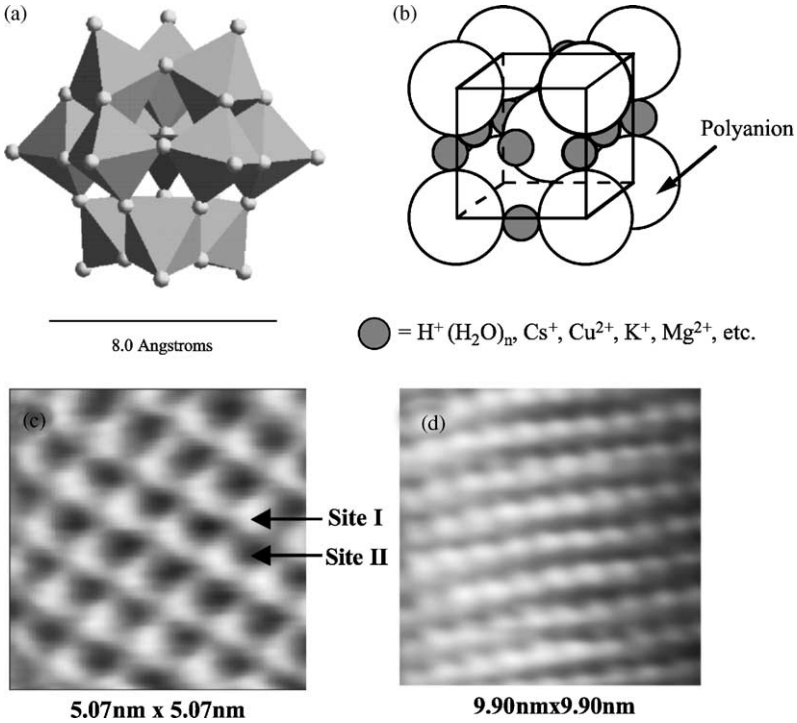

Fig. 1. (a) Polyhedral representation of the molecular structure of the quasi-spherical Keggin-type [27] $[PMo_{12}O_{40}]^{3-}$ heteropolyanion (primary structure) [26]; (b) schematic of the secondary structure of heteropolyacids [29]; (c) STM image of $H_3PMo_{12}O_{40}$ array on graphite; (d) STM image of $H_4SiW_{12}O_{40}$ array on graphite.

3. Results and discussion

3.1. Self-assembled and well-ordered monolayer arrays

Fig. 1(a) shows the molecular structure of the quasi-spherical (T_d symmetry) Keggin-type [27] $[PMo_{12}O_{40}]^{3-}$ heteropolyanion [26]. The structure of $[PMo_{12}O_{40}]^{3-}$ consists of a heteroatom, P, at the center of the anion cluster, tetrahedrally coordinated to four oxygen atoms. This tetrahedron is surrounded by twelve MoO_6 octahedra. The van der Waals diameter along the three-fold axis of symmetry (i.e. the vertical dimension of the structure in Fig. 1(a)) is 11.97 Å [26,49,50]. Fig. 1(b) shows the three-dimensional array of HPAs comprising heteropolyanions, protons, cations, water, and/or organic molecules, called the secondary structure [29]. The counter-cations are located in the interstitial spaces between heteropolyanions. The primary structure, the Keggin structure [27], of the heteropolyanion is relatively stable. However, the secondary structure is very labile and may change in different environments by either increasing or decreasing the interstitial space between heteropolyanions [29]. Fig. 1(c) and (d) shows the STM images of $H_3PMo_{12}O_{40}$ and $H_4SiW_{12}O_{40}$ samples deposited on graphite, respectively. The STM images clearly show the formation of self-assembled and well-ordered arrays on the graphite surface. The periodicities of the unit cells constructed on the basis of lattice constants determined from two-dimensional fast Fourier Transform (2D FFT) are 10.8 and 11.2 Å for $H_3PMo_{12}O_{40}$ and $H_4SiW_{12}O_{40}$ arrays, respectively, in good agreement with lattice constants of the Keggin-type HPAs obtained by STM [19–25,32,33] and X-ray crystallography [26,49,50].

Fig. 2(a) shows the typical tunneling spectra taken at two different sites, denoted as Sites I and II in the image of the $H_3PMo_{12}O_{40}$ array in Fig. 1(c). The spectrum taken at a position corresponding to the bright

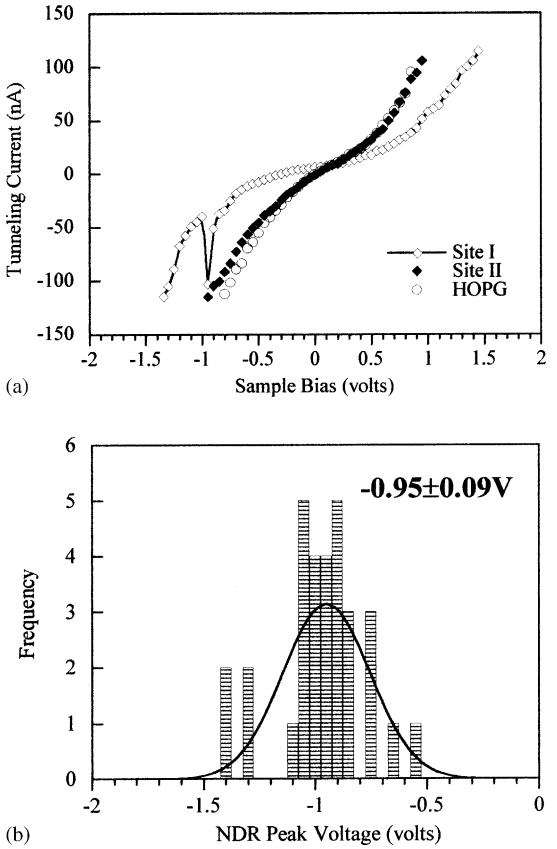

Fig. 2. (a) *I–V* spectra taken at two different sites (Sites I and II) in the STM image of $H_3PMo_{12}O_{40}$ in Fig. 1(c); (b) frequency of NDR peak voltages of $H_3PMo_{12}O_{40}$ monolayer arrays exhibiting monomodal distribution with a statistical average of -0.95 ± 0.09 V.

corrugation (Site I) exhibits a distinctive *I–V* behavior, referred to as negative differential resistance, showing a NDR peak at -0.95 V. The NDR peak voltage was defined as the voltage at which the maximum current was observed in this region. A tunneling spectrum taken at the interstitial space (Site II) between bright corrugations showed the same *I–V* response as bare graphite, indicating that the two-dimensional array of $H_3PMo_{12}O_{40}$ on graphite is a monolayer, as previously demonstrated [19–25]. The NDR measurements atop the bright corrugations (Site I) were carried out 10–30 times with at least three different tips to obtain more accurate and reproducible results, and to provide a basis for statistical analyses. Fig. 2(b) shows the distribution of NDR peak voltages of the $H_3PMo_{12}O_{40}$ sample. The average NDR peak voltage

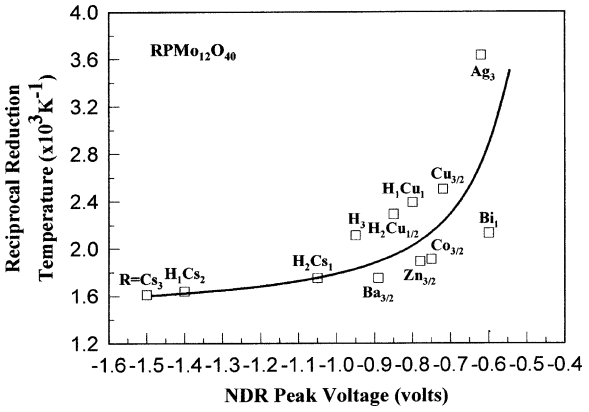

Fig. 3. Correlation between NDR peak voltage and reciprocal reduction temperature [46] of cation-exchanged $RPMo_{12}O_{40}$ ($R = H_{3-x}Cs_x$ ($x = 0$–3), $H_{3-x}Cu_{x/2}$ ($x = 0$–3), Ag_3, $Ba_{3/2}$, $Zn_{3/2}$, $Co_{3/2}$, Bi_1) HPAs.

for $H_3PMo_{12}O_{40}$ was -0.95 ± 0.09 V. The most reproducible and representative NDR peak voltage of each HPA sample examined in this work was determined in this way.

3.2. Correlation between NDR peak voltage and reduction potential

The STM measurements in this work were done at positive sample biases with respect to the tip. This means that electrons flow from tip to sample in the normal mode of operation. NDR behavior in the tunneling spectra of HPAs is observed at negative sample biases, i.e. when electrons tunnel from sample to tip. We have demonstrated that the striking NDR behavior of nanostructured HPA arrays measured by STM is closely related to the electronic properties of these materials, and may serve as a fingerprint of their redox properties [19–23]. Fig. 3 shows the correlation between NDR peak voltages of cation-exchanged HPAs and reciprocal reduction temperatures of cation-exchanged HPA samples taken from the literature [46]. It is noticeable from this result that the reduction behavior of HPAs can be correlated with their NDR peak voltages; more reducible HPAs show NDR peaks at less negative applied voltages.

Fig. 4 shows the correlation between NDR peak voltage and reduction potential of heteroatom-substituted HPAs, $H_nXW_{12}O_{40}$ (X = P(V), Si(IV), B(III),

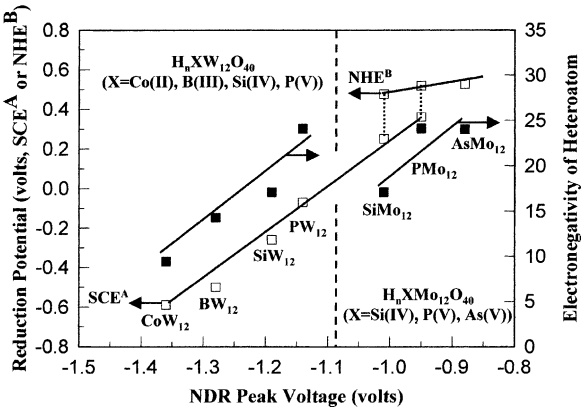

Fig. 4. Correlation between NDR peak voltage and reduction potential of heteroatom-substituted $H_nXW_{12}O_{40}$ (X = P(V), Si(IV), B(III), Co(II)) [31,51,52] and $H_nXMo_{12}O_{40}$ (X = As(V), P(V), Si(IV)) [31,45,51,52] HPAs.

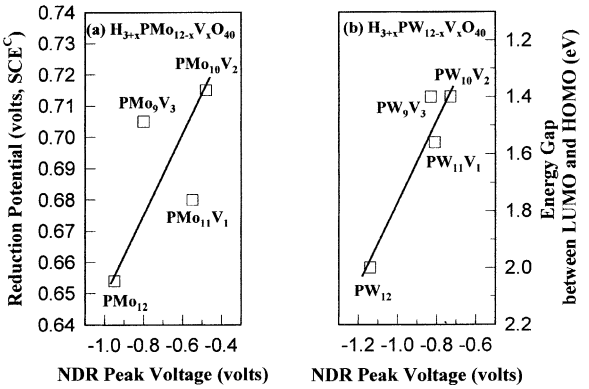

Fig. 5. (a) Correlation between NDR peak voltage and reduction potential [54] of vanadium-substituted $H_{3+x}PMo_{12-x}V_xO_{40}$ (x = 0–3) HPAs; (b) correlation between NDR peak voltage and reduction potential (energy gap between the LUMO and the HOMO) [55] of vanadium-substituted $H_{3+x}PW_{12-x}V_xO_{40}$ (x = 0–3) HPAs.

Co(II)) and $H_nXMo_{12}O_{40}$ (X = As(V), P(V), Si(IV)). Reduction potentials of $H_nXW_{12}O_{40}$ (X = P(V), Si(IV), B(III), Co(II)) HPAs determined using SCE as a reference electrode were taken from the literature [31,51,52]. Reduction potentials of $H_nXMo_{12}O_{40}$ (X = As(V), P(V), Si(IV)) HPAs determined using either NHE [45] or SCE [31,51,52] as a reference electrode were also taken from the literature. The NDR peak voltage of HPAs in both heteroatom-substituted HPA families appeared at less negative values with increasing reduction potential of the HPAs. This result supports the conclusion that more reducible HPAs show NDR behavior at less negative applied voltages in their tunneling spectra, as observed for cation-exchanged HPAs. As can be seen from the line connecting the open squares in this figure, this correlation holds across different families of heteroatom-substituted HPAs.

The correlations between NDR peak voltage and reduction potential of framework metal atom (polyatom)-substituted $H_nPW_{11}MO_{40}$ (M = W(VI), Mo(VI), V(V)) [53] and $H_3PW_{12-x}Mo_xO_{40}$ (x = 0–12) [21] HPAs have been previously demonstrated, showing that NDR peak voltages of these HPA families appeared at less negative values with increasing reduction potential of the HPAs, as consistently observed for cation-exchanged (Fig. 3) and heteroatom-substituted HPAs (Fig. 4). The reduction potentials of the polyatom-substituted $H_nPW_{11}MO_{40}$ (M = W(VI), Mo(VI), V(V)) HPAs were found to increase in the order W- < Mo- < V-containing HPA samples [29–31,53], and those of $H_3PW_{12-x}Mo_xO_{40}$ (x = 0–12) HPAs increased in a monotonic fashion with increasing numbers of Mo atoms substituted [21]. The effect of vanadium atom substitution on the NDR peak voltages and reduction potentials of $H_{3+x}PMo_{12-x}V_xO_{40}$ (x = 0–3) and $H_{3+x}PW_{12-x}V_xO_{40}$ (x = 0–3) HPAs was somewhat more complicated. Fig. 5 shows the correlation between NDR peak voltage and reduction potential of vanadium-substituted HPAs. Reduction potentials of $H_{3+x}PMo_{12-x}V_xO_{40}$ (x = 0–3) samples determined using SCE as a reference electrode were taken from a published report [54], while those of $H_{3+x}PW_{12-x}V_xO_{40}$ (x = 0–3) samples were determined from the energy gap between the lowest unoccupied molecular orbital (LUMO) and the highest occupied molecular orbital (HOMO) [55]. Interestingly, both HPA families showed the same trends of reduction potential and NDR peak voltage with respect to the number of vanadium atoms substituted. In each vanadium-substituted HPA family, however, NDR peak voltages and reduction potentials of the HPAs did not vary monotonically with the number of vanadium ions. Instead, $H_5PMo_{10}V_2O_{40}$ and $H_5PW_{10}V_2O_{40}$, which have the highest reduction potentials in each HPA family, exhibited the least negative NDR peak voltage within the families.

3.3. Dependence of NDR peak voltage and reduction potential of HPAs on the electronegativity of substituted atoms

The Tanaka electronegativity scale [56], which takes into account the electron-donating and -accepting ability of the substituted atom, has been utilized to explain the role and effect of substituted atoms on the reduction potentials and NDR peak voltages of HPAs [19–23,53]. The Tanaka electronegativity [56] is defined as $(1 + 2Z)X_o$, reflecting both charge (Z) and Pauling electronegativity (X_o). For cation-exchanged HPAs (Fig. 3), simple calculation of Tanaka electronegativity of the exchanged cation leads to the conclusion that the HPA salts with more electronegative counter-cations possess higher reduction potentials and exhibit NDR behavior at less negative applied voltages [19,21,22,53]. One explanation for this result is that a more electronegative cation acts as a large electron reservoir to facilitate electron transfer to the heteropolyanion framework in reducing environments, by providing a route for electron delocalization [57].

For heteroatom-substituted $H_nXW_{12}O_{40}$ (X = P(V), Si(IV), B(III), Co(II)) and $H_nXMo_{12}O_{40}$ (X = As(V), P(V), Si(IV)) HPAs, interestingly, Fig. 4 shows that NDR peak voltage and reduction potential dependencies on the electronegativity of heteroatoms exhibit exactly the same trends as those observed for cation-exchanged HPAs [23]; the NDR peak voltage of heteroatom-substituted HPAs appeared at less negative values with increasing reduction potential of the HPAs and with increasing electronegativity of the heteroatom. When taking into account differences in the electron-donating and -accepting ability of the heteroatoms, the role and effect of heteroatoms on the reduction potential of HPAs may be understood in a similar manner as suggested above for cation-exchanged HPAs. More importantly, Fig. 4 also shows that the correlations of NDR peak voltages with heteroatom electronegativity (closed squares) established for each HPA family are nearly parallel, suggesting that the influences of the framework composition and the heteroatom identity on the reduction potential are largely additive, as suggested by Pope [26,58].

In the case of polyatom-substituted HPAs, surprisingly, previous STM studies investigating the $H_nPW_{11}MO_{40}$ (M = W(VI), Mo(VI), V(V)) [53] and $(NH_4)_nMW_{17}O_{56}F_6NaH_4$ (M = Mn(II), Cu(II), Mn(III), Fe(III)) [59] HPAs have shown that the NDR peak voltages of HPA arrays appeared at less negative values with increasing reduction potential of the HPAs, and with decreasing electronegativity of the polyatom; the trends of polyatom electronegativity with respect to NDR peak voltage and reduction potential of polyatom-substituted HPAs are the opposite of those seen for the cation-exchanged HPAs (Fig. 3) and for heteroatom-substituted HPAs (Fig. 4). Pairs of data points such as $H_4SiW_{12}O_{40}$–$H_4SiMo_{12}O_{40}$ and $H_3PW_{12}O_{40}$–$H_3PMo_{12}O_{40}$, shown in Fig. 4 also support this trend with respect to polyatom electronegativity: tungsten is more electronegative than molybdenum, but the W-HPAs are less reducible than their Mo counterparts. A molecular orbital study [55] for $H_nPM_{12-x}V_xO_{40}$ (M = Mo(VI), W(VI); x = 0–3) HPAs has clarified the effect of polyatom electronegativity on the reduction potential of the HPAs, demonstrating that electrons added to the vanadium-substituted HPAs are localized on the less electronegative metal centers. The less electronegative vanadium atom is much more efficient in the role of electron localization [55].

3.4. NDR peak voltage as a correlating parameter for reduction potential

We have demonstrated that redox properties of HPAs can be determined from surface electronic properties of nanostructured HPA monolayers, and have established correlations between NDR peak voltage and reduction potential of HPAs, by investigating a wide set of cation-exchanged (Fig. 3), heteroatom-substituted (Fig. 4), and polyatom-substituted HPAs (Fig. 5). Within each HPA family, we observed systematic variations of NDR peak voltage and reduction potential of HPAs depending on the electronegativity of the exchanged/substituted atoms. The correlations shown in Figs. 3–5 can serve as valuable design bases to predict NDR peak voltage and reduction potential of an HPA sample, by locating the electronegativity of the exchanged/substituted atom within the correlation curve of the HPA family to which the HPA sample belongs. The most important and general conclusion derived from a series of experimental findings, regardless of exchanged/substituted positions, is that NDR peaks appeared at less negative potentials for

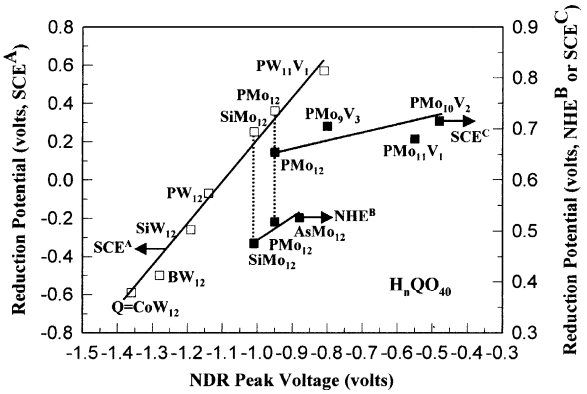

Fig. 6. Correlation between NDR peak voltage and reduction potential of HPAs with different heteroatoms and framework compositions. Except for $H_4PW_{11}V_1O_{40}$, data points shown here are from Figs. 4 and 5(a).

higher reduction potentials of the HPAs within each HPA family. This means that NDR peak voltage can probe the reduction potential of individual HPAs.

However, the correlations between NDR peak voltages and redox properties of HPAs shown in Figs. 3 and 5 are largely qualitative. Direct comparison of reduction potential of HPAs between those belonging to different HPA families, for example, between $H_4SiW_{12}O_{40}$ in Fig. 4 (heteroatom-substituted HPAs) and $H_5PMo_{10}V_2O_{40}$ in Fig. 5(a) (polyatom-substituted HPAs), is not simple, because of the lack of reduction potential data of the HPAs determined on the same measurement basis. The lack of consistent data represents a significant barrier to the use of reduction potentials from electrochemistry experiments as design parameters, especially in heterogeneous catalysis. The question is whether NDR peak voltages of HPAs can serve as a single correlating parameter for the reduction potentials of HPA spanning different HPA families, i.e. whether NDR peak voltage can serve as an alternative parameter (which is independent of solvent, electrode, etc. variations encountered in electrochemical measurements) for reduction potential of HPAs across all HPA families examined in this work. Fig. 6 provides an answer to that question. Fig. 6 shows correlations between NDR peak voltages and reduction potentials of HPAs with different heteroatoms and framework compositions (note that superscripts on the *y*-axes in Figs. 4–6 differentiate the measurement basis of the reduction potentials; the same superscript represents the same measurement basis). The open squares in Fig. 6 represent the same data as in Fig. 4, plus $H_4PW_{11}V_1O_{40}$. These data points cover a series of heteroatom-substituted ($H_nXW_{12}O_{40}$ and $H_nXMo_{12}O_{40}$) and polyatom-substituted ($H_nSiM_{12}O_{40}$ and $H_nPM_{12}O_{40}$) HPA families. Closed squares represent data shown in Figs. 4 and 5(a) for comparison purposes. Importantly, the correlation represented by the open squares clearly demonstrates that NDR peak voltages are directly correlated with reduction potentials of HPAs regardless of substituted structures. The correlating lines also provide a comparison basis for reduction potential of HPAs, even when reduction potentials of HPAs are not available on the same measurement basis from electrochemistry. For example, one can say that $H_5PMo_{10}V_2O_{40}$ has higher reduction potential than $H_4SiW_{12}O_{40}$ by considering their positions relative to a common reference, $H_3PMo_{12}O_{40}$. It is concluded that the NDR peak voltage of an HPA probes its reduction potential, and therefore, the NDR peak voltage can be utilized as a correlating parameter (or as an alternative parameter) for the reduction potential.

3.5. NDR-based selection of HPAs for propane oxidation

HPAs have been utilized commercially as catalysts for the selective oxidation of methacrolein into methacrylic acid [60], and as co-catalysts for the vapor-phase oxidation of ethylene to acetic acid [61,62]. They have also been investigated in laboratories as catalysts for the Wacker-type oxidation of *n*-butene [63], and for the selective oxidation of isobutane into methacrylic acid and methacrolein [64]. HPAs are among a relatively small group of catalytic materials that are able to promote the direct oxidation of propane into acrylic acid. The methacrolein oxidation catalyst is a vanadium-containing phosphomolybdate modified with small amounts of copper, cesium, and one or more additional promoter elements from group V such as arsenic, antimony and bismuth. Similarly, a family of $H_{3+x}PMo_{12-x}V_xO_{40}$ ($x = 0$–3) HPAs has been investigated as selective oxidation catalysts for propane oxidation.

Fig. 7 shows the correlation between NDR peak voltage of $H_{3+x}PMo_{12-x}V_xO_{40}$ ($x = 0$–3) HPAs and acrylic acid yield [65,66] over the

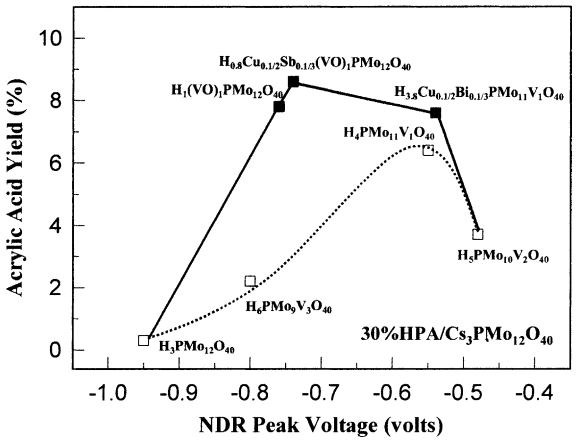

Fig. 7. Acrylic acid yields over $H_{3+x}PMo_{12-x}V_xO_{40}$ ($x = 0$–3)/$Cs_3PMo_{12}O_{40}$ (open squares) and HPAs (with vanadyl and/or promoting cation groups)/$Cs_3PMo_{12}O_{40}$ (closed squares), plotted as a function of NDR peak voltage of the HPAs. Oxidations were carried out by first activating the catalyst by flowing 1 atm of a propane/air mixture (52.5/38 ml/min) at 350 °C, then carrying out the oxidation by continuously passing a propane/air/nitrogen mixture (3.2/15/16 ml/min) over 4 ml of the catalyst (30% HPA/$Cs_3PMo_{12}O_{40}$ having a medium pore radius of ~120 Å) at 375–380 °C [65,66]. The lines in the figure connect available data points, and are not meant to imply that the highest yield catalysts examined to date necessarily represent maxima in the yield vs. NDR potential correlations.

$H_{3+x}PMo_{12-x}V_xO_{40}$ ($x = 0$–3) HPAs supported on $Cs_3PMo_{12}O_{40}$ in propane oxidation (open squares). Propane oxidation was carried out with a feed containing a slight excess of propane at a given condition. It is generally preferable for commercial purposes to minimize recycle and reactor size, and therefore, to run reactions with propane and oxygen ratios close to their stoichiometric ratios (1:2). Under stoichiometric conditions, it was observed that unsupported $H_{3+x}PMo_{12-x}V_xO_{40}$ ($x = 0$–3) HPAs had short lifetimes of approximately 2 h [65,66]. Although the catalytic performance of $H_{3+x}PMo_{12-x}V_xO_{40}$ ($x = 0$–3) HPAs was enhanced by supporting them on SiO_2 under conditions of high propane excess, the SiO_2-supported catalysts offered only a minor improvement under practical stoichiometric conditions [65,66]. Recent works [67,68] have shown that the cesium-containing HPAs efficient for propane oxidation are, in fact, catalytically active HPAs supported on inactive cesium salts of HPAs. Some protonic character is needed for the $H_{3-x}Cs_x$-exchanged HPAs to be catalytically active, since $H_{3-x}Cs_xPMo_{12}O_{40}$ ($x \neq 3$) has modest activity for propane oxidation and some acrylic acid is produced, while pure $Cs_3PMo_{12}O_{40}$ has little or no activity. When a $H_{3+x}PMo_{12-x}V_xO_{40}$ ($x = 0$–3) HPA was supported on an inactive $Cs_3PMo_{12}O_{40}$, better catalytic performance was obtained than for the corresponding HPA supported on SiO_2 [66]. The pore size distribution of the $Cs_3PMo_{12}O_{40}$ has a pronounced effect on the catalytic performance, with the best AA yield and selectivity resulting from catalysts having the maximum number of large (<100 Å) pores and minimum concentration of small pores which can lead to burning of reactants and/or products [43,48,69]. Under more practical stoichiometric conditions, $Cs_3PMo_{12}O_{40}$-supported HPAs were found to be more stable than the unsupported HPAs and to have lifetimes of approximately 200 h [66]. The correlation between NDR peak voltage and acrylic acid yield shown in Fig. 7 (open squares) provides some insights into the design/selection basis of HPAs efficient for propane oxidation; NDR peak voltage can be utilized as a prediction tool for catalytic performance, and there exists an optimum range of NDR peak voltage for highest AA yield. In searching for possible HPA candidates producing enhanced AA yields, correlation curves shown in Figs. 3–6 may provide valuable design and selection information.

It was recently reported that $Cs_{2x}(NH_4)_{6-2x}(VO)_1[PMo_{11}V_1(IV)O_{40}][PMo_{12}O_{40}]$ ($0 \leq x \leq 3$), which was formed by thermal exchange of cesium for ammonium cations in $(NH_4)_5[PMo_{11}V_1(IV)O_{40}]$, was active for oxidative dehydrogenation of isobutyric acid into methacrylic acid [70]. Another recent study [71] investigating transient responses of the local electronic and geometric structures of $H_{3+x}PMo_{12-x}V_xO_{40}$ catalysts in selective oxidations showed that the vanadium migrated out of the Keggin anion into the cation-exchange position upon thermal treatment and/or chemical reduction (during performance of vapor-phase oxidations), producing a lacunary species characterized by defects in the number of metal–oxygen octahedra. That work [71] also concluded that the active state of the HPA was a partially reduced oligomer of polyanions bridged by vanadyl groups. These results open the possibility that an HPA with vanadyl group positioned initially and intentionally in the cation-exchange position might be

an active catalyst in the vapor-phase oxidation. Such incorporation of vanadium is expected to cause an increase in reduction potential and improvement of catalytic performance. Other promoting cation groups that increase the reduction potential may also enhance catalytic performance. Fig. 7 also shows the relationship between NDR peak voltage of HPAs and AA yield over HPAs/$Cs_3PMo_{12}O_{40}$ in propane oxidation, established for HPAs with vanadyl and/or promoting cation groups (closed squares). The correlation shows that substitution of protons with vanadyl and/or more electronegative (promoting) cations shifted NDR peak voltages of HPAs to less negative values, and accordingly, increased AA yields over the HPAs. These results demonstrate that NDR peak voltage predicts catalytic performance of the HPAs in propane oxidation, and that an optimum range of NDR peak voltage is required in order for an HPA to show pronounced catalytic performance in the reaction. These results also suggest that HPAs can be rationally designed/selected on the basis of NDR peak voltage as efficient catalysts for propane oxidation.

While the correlation of acrylic acid yields with NDR peak voltages in Fig. 7 exhibits volcano behavior, we do not mean to suggest that such correlations might be expected only for yield data, or that one should necessarily expect to find a volcano in most cases. For a single reaction, one might expect to find a monotonic correlation of catalyst *activity* with NDR peak potential. For a purely sequential oxidation process in which the desired product is subject to over-oxidation, one might expect to find such a "volcano" plot for *yield* versus catalyst reduction potential, provided that the range of catalysts spanned that from low activity but high selectivity, to high activity but low selectivity. If the catalysts considered all lie to one side of the optimum reduction potential (or NDR peak voltage) then one would only observe monotonically upward or downward trends when attempting such correlations. If parallel, unselective

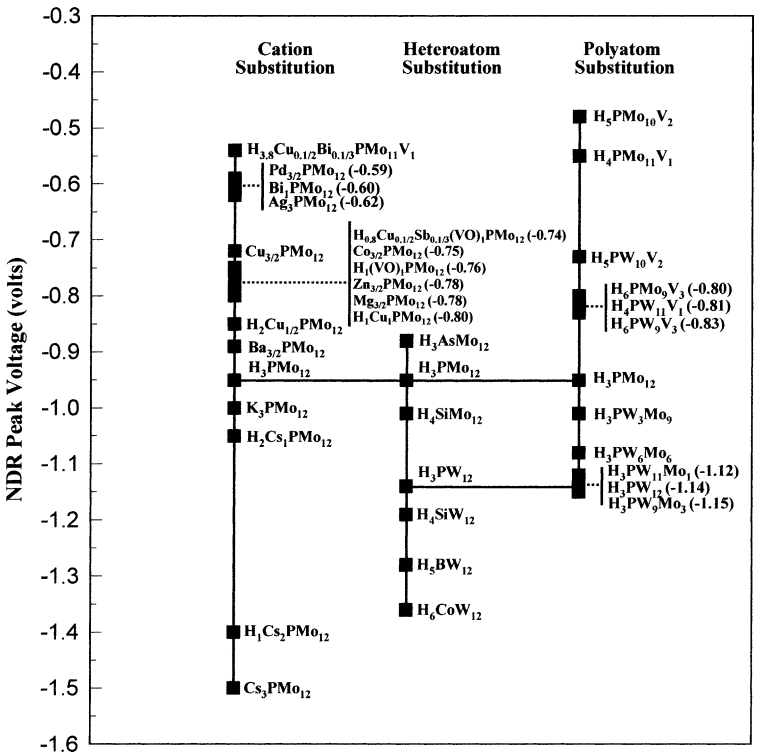

Fig. 8. Map of NDR peak voltages established for Keggin-type HPAs, along with classification according to the exchanged/substituted position.

oxidation processes also compete with the desired reaction, then correlations of reaction *selectivity* with reduction potential may provide more useful insights. We do not argue that Fig. 7 is a representative pattern for all HPA-catalyzed oxidations, but rather that the comprehensive scale of NDR peak voltages for these compounds provides a new opportunity to explore the variety of useful predictions and correlations that might be developed with these molecular catalysts.

To that end, Fig. 8 shows the map of NDR peak voltages established for all HPAs examined in this work, along with classification according to the exchanged/substituted position. The map can provide a basis in searching for possible HPA candidates for different selective oxidations. The tunability of NDR peak voltage, i.e. reduction potential, of HPAs depending on exchanged/substituted atoms and positions makes it possible for HPAs be chosen in a systematic way. This work demonstrates that NDR peak voltage of HPAs, which is an alternative parameter for their reduction potential, serves as a selection, prediction, and design basis in searching for HPAs efficient for propane oxidation, and suggests applications to many other catalytic oxidation processes.

4. Conclusions

STM investigation of surface electronic properties of nanostructured HPA monolayers was carried out to relate nanoscale properties to catalytic properties of HPAs. Keggin-type HPAs with different counter-cation, polyatom, and heteroatom substitutions were examined for this purpose. All HPA samples studied in this work formed well-ordered monolayer arrays, and exhibited NDR behavior in their tunneling spectra. The observed NDR peak voltages were correlated with the reduction potentials of HPAs. Across all HPA families, it was consistently observed that more reducible HPAs show NDR behavior at less negative applied voltages. NDR peak voltage could be utilized as a correlating parameter (or as an alternative parameter) for the reduction potentials of HPAs; less negative NDR peak voltages correspond to higher reduction potentials of HPAs. A “volcano” plot constructed by relating NDR peak voltage to catalytic performance of HPAs for propane selective oxidation showed that there was an optimum range of NDR peak voltage for the best performance in the reaction. This work successfully demonstrates that NDR peak voltage of HPAs can serve as a selection, prediction, and design basis in searching for HPAs efficient for selective propane oxidation. A map of NDR peak voltages of HPAs was established to provide a design and selection basis of HPA for selective oxidation. The tunability of NDR peak voltages of HPAs depending on exchanged/substituted atoms and positions in a systematic way makes it possible for HPAs be rationally designed as efficient oxidation catalysts.

Acknowledgements

The authors thank Prof. C.L. Hill at Emory University and Dr. K. Kourtakis at E.I. duPont de Nemours and Company for providing several of the HPA samples. In K. Song acknowledges fellowship support from the Seoam Scholarship Foundation.

References

[1] D.L. Carroll, R. Czerw, D. Tekeleab, D.W. Smith Jr., Langmuir 16 (2000) 3574.
[2] F.M. Leibsle, P.W. Murray, N.G. Condon, G. Thornton, J. Appl. Phys. D 30 (1997) 741.
[3] P. Cernota, K. Rider, H.A. Yoon, M. Salmeron, G.A. Somorjai, Surf. Sci. 445 (2000) 249.
[4] H.J. Lee, W. Ho, Phys. Rev. B 61 (2000) R16347.
[5] A. Steltenpohl, N. Memmel, Surf. Sci. 443 (1999) 13.
[6] B.C. Stipe, M.A. Rezaei, W. Ho, S. Gao, M. Persson, B.I. Lundqvist, Phys. Rev. Lett. 78 (1997) 4410.
[7] Q. Chen, C.C. Perry, B.G. Frederick, P.W. Murray, S. Haq, N.V. Richardson, Surf. Sci. 446 (2000) 63.
[8] P. Cernota, H.A. Yoon, M. Salmeron, G.A. Somorjai, Surf. Sci. 415 (1998) 351.
[9] S.L. Silva, A.A. Patel, T.M. Pham, F.M. Leibsle, Surf. Sci. 441 (1999) 351.
[10] J.J. Boland, J.S. Villarrubia, Science 248 (1990) 838.
[11] P.T. Wouda, B.E. Nieuwenhuys, M. Schmid, P. Varge, Surf. Sci. 359 (1996) 17.
[12] K.W. Hipps, X. Lu, X.D. Wang, U. Mazur, J. Phys. Chem. 100 (1996) 11207.
[13] M.K.-J. Johansson, S.M. Gray, L.S.O. Johansson, J. Vac. Sci. Technol. B 14 (1996) 1015.
[14] B.C. Stipe, M.A. Rezaei, W. Ho, Science 280 (1998) 1732.
[15] H.-J. Müssig, D. Krüger, S. Hinrich, P.O. Hansson, Surf. Sci. 314 (1994) L884.
[16] A.G. Petukhov, D.O. Demchenko, A.N. Chantis, J. Vac. Sci. Technol. B 18 (2000) 2109.

[17] C. Zeng, H. Wang, B. Wang, J. Yang, J.G. Hou, Appl. Phys. Lett. 77 (2000) 3595.
[18] C.B. Gorman, R.L. Carroll, R.R. Fuierer, Langmuir 17 (2001) 6923.
[19] M.S. Kaba, I.K. Song, M.A. Barteau, J. Phys. Chem. 100 (1996) 19577.
[20] M.S. Kaba, I.K. Song, M.A. Barteau, J. Vac. Sci. Technol. A 15 (1997) 1299.
[21] I.K. Song, M.S. Kaba, M.A. Barteau, W.Y. Lee, Catal. Today 44 (1998) 285.
[22] M. Kinne, M.A. Barteau, Surf. Sci. 447 (2000) 105.
[23] I.K. Song, R.B. Shnitser, J.J. Cowan, C.L. Hill, M.A. Barteau, Inorg. Chem. 41 (2002) 1292.
[24] I.K. Song, M.S. Kaba, M.A. Barteau, J. Phys. Chem. 100 (1996) 17528.
[25] M.S. Kaba, M.A. Barteau, W.Y. Lee, I.K. Song, Appl. Catal. A 194 (2000) 129.
[26] M.T. Pope, Heteropoly and Isopoly Oxometalates, Springer, New York, 1983.
[27] J.F. Keggin, Nature 131 (1933) 908.
[28] R. Neumann, Prog. Inorg. Chem. 47 (1998) 317.
[29] M. Misono, Catal. Rev. Sci. Eng. 29 (1987) 269.
[30] I.V. Kozhevnikov, Catal. Rev. Sci. Eng. 37 (1995) 311.
[31] T. Okuhara, N. Mizuno, M. Misono, Adv. Catal. 41 (1996) 113.
[32] I.K. Song, M.S. Kaba, G. Coulston, K. Kourtakis, M.A. Barteau, Chem. Mater. 8 (1996) 2352.
[33] M.S. Kaba, I.K. Song, D.C. Duncan, C.L. Hill, M.A. Barteau, Inorg. Chem. 37 (1998) 398.
[34] A.M. Dykhne, S.Y. Vasil'ev, O.A. Petrii, A.G. Rudavets, G.A. Tsirlina, Dokl. Akad. Nauk. 368 (1999) 467.
[35] M.S. Kaba, I.K. Song, M.A. Barteau, J. Phys. Chem. B 106 (2002) 2337.
[36] C. Centi, F. Trifirò, in: Proceedings of the First Tokyo Conference on Advance Catalysis Science and Technology, Tokyo, Japan, 1990, p. 225.
[37] M.M. Lin, Appl. Catal. A 207 (2001) 1.
[38] K. Ushikubo, H. Kinoshita, A. Watanabe, JP10 45,665 (1998).
[39] X. Tu, M. Takahashi, M. Furuta, H. Nizuma, US Patent 6,291,393 (2001).
[40] M. Ai, Catal. Today 13 (1992) 679.
[41] W. Ueda, Y. Suzuki, W. Lee, S. Imaoka, Stud. Surf. Sci. Catal. 101 (1996) 1065.
[42] N. Mizuno, M. Tateishi, M. Iwamoto, Appl. Catal. A 128 (1995) L165.
[43] J.E. Lyons, A.F. Volpe Jr., P.E. Ellis Jr., S. Karmakar, US Patent 5,990,348 (1999).
[44] T. Ushikubo, JP10 45,643 (1998).
[45] K. Eguchi, T. Seiyama, N. Yamazoe, S. Katsuki, H. Taketa, J. Catal. 111 (1988) 336.
[46] M. Ai, Appl. Catal. 4 (1982) 245.
[47] T. Okuhara, T. Nishimura, H. Watanabe, M. Misono, J. Mol. Catal. 74 (1994) 247.
[48] T.P. Wijesekera, J.E. Lyons, P.E. Ellis Jr., US Patent 6,169,202 (2001).
[49] G.M. Brown, M.R. Noe-Spirlet, W.R. Busing, H.A. Levy, Acta Cryst. B 33 (1977) 1038.
[50] H. Hayashi, J.B. Moffat, J. Catal. 77 (1982) 473.
[51] J.J. Alternau, M.T. Pope, R.A. Prados, H. So, Inorg. Chem. 14 (1975) 417.
[52] M. Sadakane, E. Steckhan, Chem. Rev. 98 (1998) 219.
[53] I.K. Song, M.A. Barteau, J. Mol. Catal. A 182–183 (2002) 185.
[54] I.V. Kozhevnikov, E.G. Zhizhina, N.B. Kuznetsova, Kinet. Katal. 56 (1987) 811.
[55] R.S. Weber, J. Phys. Chem. 98 (1994) 2999.
[56] K. Tanaka, A. Ozami, J. Catal. 8 (1967) 1.
[57] H.C. Kim, S.H. Moon, W.Y. Lee, Chem. Lett. (1991) 447.
[58] M.T. Pope, A. Müller, Angew. Chem. Int. Ed. 30 (1991) 34.
[59] M.S. Kaba, I.K. Song, S.H. Wasfi, M.A. Barteau, J. Electrochem. Soc. 149 (2002) E117.
[60] N. Shimizu, Petrotechniques 6 (1983) 778.
[61] K. Sano, H. Uchida, S. Wakabayashi, Catal. Surv. Jpn. 3 (1999) 55.
[62] T. Suzuki, H. Yoshikawa, K. Abe, K. Sano, US Patent 5,405,996 (1995).
[63] A.W. Stobbe-Kreemers, R.B. Dielis, M. Makkee, J.J.F. Scholten, J. Catal. 154 (1995) 175.
[64] N. Mizuno, T. Tateishi, M. Iwamoto, J. Chem. Soc. Chem. Commun. (1994) 1411.
[65] J.E. Lyons, P.E. Ellis Jr., S. Karmakar, S.N. Shaikh, US Patent 5,705,685 (1998).
[66] S. Karmakar, A.F. Volpe Jr., P.E. Ellis Jr., J.E. Lyons, US Patent 6,043,184 (2000).
[67] A.F. Volpe Jr., J.E. Lyons, P.E. Ellis Jr., S. Karmakar, Prepr. Am. Chem. Soc., Div. Petrol. Chem. 44 (1999) 156.
[68] M. Langpape, M. Millet, U. Ozkan, M. Boudeulle, J. Catal. 181 (1999) 80.
[69] T.P. Wijesekera, J.E. Lyons, P.E. Ellis Jr., US Patent 6,060,419 (2000).
[70] C. Marchal-Roch, N. Laronze, N. Cuillou, A. Tézé, G. Hervé, Appl. Catal. A 203 (2000) 143.
[71] J.K. Lee, J. Melsheimer, S. Berndt, G. Mestl, R. Schlögl, K. Köhler, Appl. Catal. A 214 (2001) 125.